Recombinant Subgroup B Human Respiratory Syncytial Virus Expressing Enhanced Green Fluorescent Protein Efficiently Replicates in Primary Human Cells and Is Virulent in Cotton Rats

Lemon, K., Nguyen, D. T., Ludlow, M., Rennick, L. J., Yüksel, S., van Amerongen, G., ... Duprex, W. P. (2015). Recombinant Subgroup B Human Respiratory Syncytial Virus Expressing Enhanced Green Fluorescent Protein Efficiently Replicates in Primary Human Cells and Is Virulent in Cotton Rats. Journal of Virology, 89(5), 2849-2856. DOI: 10.1128/JVI.03587-14

Published in:
Journal of Virology

Document Version:
Publisher's PDF, also known as Version of record

JVI Journals.ASM.org

Recombinant Subgroup B Human Respiratory Syncytial Virus Expressing Enhanced Green Fluorescent Protein Efficiently Replicates in Primary Human Cells and Is Virulent in Cotton Rats

Ken Lemon,[a] D. Tien Nguyen,[b] Martin Ludlow,[c] Linda J. Rennick,[c] Selma Yüksel,[b] Geert van Amerongen,[b] Stephen McQuaid,[c] Bert K. Rima,[a] Rik L. de Swart,[b] W. Paul Duprex[d]

School of Medicine, Dentistry and Biomedical Sciences, The Queen's University of Belfast, Belfast, Northern Ireland, United Kingdom[a]; Department of Viroscience, Erasmus MC, Rotterdam, the Netherlands[b]; Tissue Pathology, Belfast Health and Social Care Trust, The Queen's University of Belfast, Belfast, Northern Ireland, United Kingdom[c]; Department of Microbiology, Boston University School of Medicine, Boston, Massachusetts, USA[d]

ABSTRACT

Human respiratory syncytial virus (HRSV) is the most important viral cause of severe respiratory tract disease in infants. Two subgroups (A and B) have been identified, which cocirculate during, or alternate between, yearly epidemics and cause indistinguishable disease. Existing *in vitro* and *in vivo* models of HRSV focus almost exclusively on subgroup A viruses. Here, a recombinant (r) subgroup B virus (rHRSV^{B05}) was generated based on a consensus genome sequence obtained directly from an unpassaged clinical specimen from a hospitalized infant. An additional transcription unit containing the gene encoding enhanced green fluorescent protein (EGFP) was introduced between the phosphoprotein and matrix genes (position 5) of the genome to generate rHRSV^{B05}EGFP(5). The recombinant viruses replicated efficiently in both HEp-2 cells and in well-differentiated normal human bronchial cells grown at air-liquid interface. Intranasal infection of cotton rats (*Sigmodon hispidus*) resulted in high numbers of EGFP$^+$ cells in epithelia of the nasal septum and conchae. When administered in a relatively large inoculum volume, the virus also replicated efficiently in bronchiolar epithelial cells and spread extensively in both the upper and lower respiratory tracts. Virus replication was not observed in ciliated epithelial cells of the trachea. This is the first virulent rHRSV strain with the genetic composition of a currently circulating wild-type virus. *In vivo* tracking of infected cells by means of EGFP fluorescence in the absence of cytopathic changes increases the sensitivity of virus detection in HRSV pathogenesis studies.

IMPORTANCE

Virology as a discipline has depended on monitoring cytopathic effects following virus culture *in vitro*. However, wild-type viruses isolated from patients often do not cause significant changes to infected cells, necessitating blind passage. This can lead to genetic and phenotypic changes and the generation of high-titer, laboratory-adapted viruses with diminished virulence in animal models of disease. To address this, we determined the genome sequence of an unpassaged human respiratory syncytial virus from a sample obtained directly from an infected infant, assembled a molecular clone, and recovered a wild-type recombinant virus. Addition of a gene encoding enhanced green fluorescent protein allowed this wild-type virus to be tracked in primary human cells and living animals in the absence of significant cytopathic effects. Imaging of fluorescent cells proved to be a highly valuable tool for monitoring the spread of virus and may help improve assays for evaluating novel intervention strategies.

Human respiratory syncytial virus (HRSV) is the most important viral cause of respiratory tract disease in infants (1). HRSV infections are observed during seasonal outbreaks in winter or during the rainy season in the tropics (2). The virus usually causes a self-limiting upper respiratory tract (URT) infection, resulting in rhinorrhea and other common cold-like clinical signs (3). However, in a minority of cases the infection can also spread to the lower respiratory tract (LRT), resulting in severe pneumonia or bronchiolitis. Risk factors for developing severe LRT infections include prematurity, pulmonary or cardiac disease, compromised immunity, and old age (4). Current treatment options are limited, although a monoclonal antibody directed against the fusion (F) glycoprotein has been developed for prophylactic use (5). Despite significant efforts in vaccine development over the past 50 years, no HRSV vaccines are currently licensed (6). Limited availability of natural animal models of disease adds to the challenge of developing vaccines and antivirals.

HRSV is a member of the family *Paramyxoviridae*, subfamily *Pneumovirinae*, genus *Pneumovirus* (1). It is an enveloped virus with a negative-sense, single-stranded RNA genome containing 10 transcription units. The glyco- (G) proteins facilitate virus attachment and entry (1, 7), and the F glycoprotein is an important target of virus neutralizing antibodies (8). Molecular epidemiological studies have identified two HRSV subgroups (A and B),

Received 1 October 2014 **Accepted** 16 December 2014

Accepted manuscript posted online 24 December 2014

Citation Lemon K, Nguyen DT, Ludlow M, Rennick LJ, Yüksel S, van Amerongen G, McQuaid S, Rima BK, de Swart RL, Duprex WP. 2015. Recombinant subgroup B human respiratory syncytial virus expressing enhanced green fluorescent protein efficiently replicates in primary human cells and is virulent in cotton rats. J Virol 89: 2849–2856. doi:10.1128/JVI.03587-14.

Editor: A. García-Sastre

Address correspondence to W. Paul Duprex, pduprex@bu.edu.

K.L. and D.T.N. contributed equally to this article.

doi:10.1128/JVI.03587-14

which cause indistinguishable disease and cocirculate during, or alternate between, yearly outbreaks (9, 10).

An improved understanding of HRSV pathogenesis would facilitate the development of novel intervention strategies. This requires virulent, well-characterized virus strains of known provenance, which can be evaluated in disease-relevant *in vitro* and *in vivo* model systems. Well-differentiated (wd) normal human bronchial epithelial (wd-NHBE) cultures grown at air-liquid interface (ALI) have been identified as a useful *in vitro* model for HRSV as they contain ciliated cells which are natural HRSV targets (11–13). Such cells provide a valuable bridge from *in vitro* to *in vivo* studies. Cotton rats represent a highly susceptible small-animal model for HRSV pathogenesis studies (14). Recently, adult human volunteers were infected with wild-type A strains to assess the effectiveness of HRSV antivirals (15–17). Irrespective of the approach used, it is critical to use naturally circulating viruses to ensure that study outcomes can be correlated with clinical outcomes. A long-standing challenge in virology is that clinical isolates often fail to cause overt cytopathic effect (CPE) in primary cells and *in vivo*; thus, infected cells must be stained to monitor the infection. This is challenging *in vitro* and magnified *in vivo* when low numbers of infected cells are present in tissues, which must be examined using ultrathin sections. These challenges have been addressed by generating recombinant (r) viruses from clinical samples and engineering them to express fluorescent proteins from an additional transcription unit (ATU), permitting novel insights into viral pathogenesis and targeted pathological assessment in appropriate cell lines and animal models (18). To extend these studies, we obtained the genome sequence of HRSV^{B05}, a wild-type subgroup B strain. Assembly of a full-length molecular clone allowed the recovery of recombinant HRSV^{B05} (rHRSV^{B05}) and insertion of an ATU containing the enhanced green fluorescent protein (EGFP) open reading frame (ORF) at position 5 between the phosphoprotein (P) and matrix (M) genes led to the generation of rHRSV^{B05}EGFP(5). We characterized rHRSV^{B05} and rHRSV^{B05}EGFP(5) *in vitro* and show that it is virulent *in vivo*.

MATERIALS AND METHODS

Determination of a complete HRSV subtype B genomic sequence directly from clinical material. Deidentified clinical material was kindly provided by Peter Coyle (Royal Victoria Hospital, Belfast, Northern Ireland). The sample was obtained from a tracheal rinse of an HRSV-positive infant during the 2004-2005 HRSV season (HRSV^{B05}). Total RNA was extracted from clinical material (500 μl) using TRIzol LS reagent (Life Technologies). First-strand cDNA was generated using a SuperScript III first-strand synthesis system (Life Technologies) and negative-sense gene-specific primers based on conserved regions of the HRSV subtype B genome. PCR primers were designed to amplify the complete viral genome in six overlapping fragments. PCR was performed on the cDNA using Phusion High-Fidelity DNA Polymerase (New England BioLabs). PCR products were purified using a QIAquick PCR purification kit (Qiagen) and sequenced using primers spanning the viral genome. Sequences were assembled, and a consensus was determined using Lasergene, version 10 (DNASTAR). Primer sequences are available on request. rgRSV is a recombinant virus based on HRSV strain A2 (HRSV^{A2}), which expresses GFP from an ATU present at position 1 (promoter proximal of the genome (19).

Construction of rHRSV^{B05} minigenomic and antigenomic plasmids. An HRSV minigenome plasmid, p(−)HRSV^{B05}DI-EGFP, contained an EGFP open reading frame (ORF) flanked by the viral 3′ and 5′ termini and preceded upstream by a T7 promoter, guanine trinucleotide, and ribozyme and followed downstream by a hepatitis delta virus ribozyme and T7 terminator sequences. A negative-sense viral RNA was produced upon transcription by T7 RNA polymerase. The minigenome construct was synthesized by GeneArt Gene Synthesis (Life Technologies) and ligated into a modified pBluescript vector (20). HRSV N, P, M2-1, and L expression plasmids were constructed in pCG(MPBS) (21). A full-length, antigenomic HRSV plasmid, pHRSV^{B05}, was constructed following restriction enzyme digestion and sequential ligation into the modified pBluescript vector (20). The viral genome sequence was orientated with respect to the T7 promoter to produce an antigenomic RNA upon transcription. The full-length HRSV plasmid was modified to contain an ATU encoding EGFP located between the P and M genes, pHRSV^{B05}EGFP(5).

Development of a minigenome assay and recovery of rHRSV. Confluent HEp-2 cells (ATCC, CCL-23) were infected with recombinant vaccinia virus MVA-T7 for 1 h at 37°C. Inoculum was aspirated, and Lipofectamine 2000 (Life Technologies) was used to transfect plasmid mixtures containing N, P, M2-1, L, and full-length or minigenome constructs. After 18 h the transfection mix was removed and replaced with OptiMEM (2 ml) (Life Technologies) containing 2% (vol/vol) fetal bovine serum (FBS). Cells were incubated for up to 7 days at 37°C with 5% (vol/vol) CO_2. Supernatants from cells transfected with full-length constructs were used to infect fresh HEp-2 monolayers, and the presence of virus was confirmed by immuno-plaque assay, fluorescence, or CPE observed by phase-contrast microscopy. Cells, transfected with the HRSV minigenome construct, were observed daily by fluorescence microscopy to detect EGFP expression. Virus stocks were prepared in HEp-2 cells. Virus titers were determined by endpoint titration in HEp-2 cells.

***In vitro* infection assays and virus characterization.** Growth kinetics was assessed by infection of HEp-2 cells at a multiplicity of infection (MOI) of 0.1. Triplicate samples were scraped, sonicated, and centrifuged to remove cellular fragments; the supernatant was snap-frozen as cell-free virus stock. Virus present in the sample for each time point was determined by endpoint titration in HEp-2 cells. Titers are expressed as 50% tissue culture infectious doses ($TCID_{50}$) calculated by the Reed and Muench method (22). To determine glycosaminoglycan (GAG) indices, CHO cells expressing GAG or GAG-deficient cells were infected and analyzed by flow cytometry (23). wd-NHBE cells were cultured in 12-mm/0.4-μm-pore-size inserts (Corning) at ALI (24). The apical surfaces of cells (estimated to contain 10^5 cells exposed at the surface) were infected at 25 to 26 days after growth at ALI. After 1 h of incubation at 37°C, inoculum was removed, and the apical surfaces were washed three times with Dulbecco's phosphate-buffered saline (DPBS) (500 μl). At 2 days postinfection (d.p.i.), DPBS (500 μl) was added to the apical compartment, and the cells were incubated at 37°C. After 10 min the DPBS and growth medium were harvested from the apical and basolateral compartments, respectively, for virus isolations and quantitative PCR (qPCR). Subsequently, automated whole-well scans were made by confocal laser scanning microscopy (CLSM) with an LSM700 system fitted on an Axio Observer Z1 inverted microscope (Zeiss), followed by semiautomated enumeration of EGFP-positive ($EGFP^+$) cells (DotCount; MIT, Boston, MA). Viruses were titrated in HEp-2 cells using 10-fold (growth kinetics) or 3-fold (apical rinse) dilutions in flat-bottom 96-well plates and cultured for 5 to 7 days at 37°C. The presence of HRSV genomes in samples was determined by TaqMan reverse transcription-PCR (RT-PCR) as previously described (25) with slight modifications. A quantified positive control for HRSV B (Vircell) was added to express the results in genome equivalents. The cycle threshold (C_T) value was calculated automatically when the fluorophore signal (6-carboxyfluorescein [FAM] for HRSV A and tetramethylrhodamine [TAMRA] for HRSV B) was detected above the background level and was used to give a quantitative indication of viral copy numbers. All *in vitro* experiments were performed at least three times. Statistical analyses were performed with SPSS, version 20.0.

HRSV immuno-plaque assay. Serial 10-fold dilutions of HRSV were prepared in OptiMEM. Confluent HEp-2 cells cultured in 24-well plates were infected with each dilution (200 μl) for 1 h at 37°C. Inoculum was aspirated, and 0.8% carboxy-methylcellulose (2 ml) (Sigma), in OptiMEM containing 2% (vol/vol) FBS, was added. Overlay medium was removed at 4 to 5 d.p.i., and cells were fixed in cold 80% (vol/vol) methanol for 1 h at 4°C. Plates were washed in distilled water and blocked with 5% (wt/vol) milk for 30 min. Goat anti-HRSV (Ab20745-1; Abcam) diluted 1:100 in blocking solution (200 μl) was added. Following 1 h of incubation at room temperature with rocking, plates were washed in distilled water, and rabbit anti-goat horseradish peroxidase (HRP) conjugate (Ab6741; Abcam) diluted 1:100 in blocking solution (200 μl) was added. Following 1 h of incubation at room temperature, plates were rinsed, and binding of the HRP-conjugated antibody was detected using 4-chloro-1-naphthol (200 μl), which was converted to produce a gray/black pigment (Pierce).

***In vivo* infection experiment.** Six groups of six female, 3- to 4-week-old cotton rats were infected intranasally with 10^4 $TCID_{50}$ of rHRSV in an inoculum volume of 10 μl or 100 μl to target the URT or LRT predominantly (26). Animals ($n = 3$/group) were euthanized by exsanguination at 4 or 6 d.p.i. The right lung was inflated with 2% (wt/vol) agarose (Sigma-Aldrich), sliced, and submerged in medium (27). Postmortem nasopharyngeal washings were collected, and the left lung was prepared for qPCR. Nasal concha, nasal septum, and agarose-inflated right lung (27) were screened and scored for microscopic fluorescence (AxioVert 25; Zeiss). Mann-Whitney U tests were used to compare differences between groups, and a P value of ≤ 0.05 was considered statistically significant.

Immunohistochemical (IHC) analysis of formalin-fixed tissues. Paraffin-embedded tissues were processed as previously described (28). HRSV-infected cells were detected using a polyclonal rabbit antibody to EGFP (Invitrogen). All fluorescently stained slides were assessed, and digital fluorescent images were acquired with a Leica DF digital camera using Leica FW4000 software.

Confocal laser scanning microscopy. Nasal tissues and agarose-inflated lung slices were fixed with phosphate-buffered saline (PBS) containing 4% (wt/vol) paraformaldehyde, permeabilized with PBS containing 0.1% (vol/vol) Triton X-100 for 30 min, counterstained with the far-red nuclear counterstain TO-PRO3 (Invitrogen) or 4′,6′-diamidino-2-phenylindole (DAPI; Vectashield), and directly analyzed for EGFP fluorescence by an LSM700 system (Zeiss) or Leica SP5 microscope (Leica Microsystems). Three-dimensional (3D) images and movies were generated using Zen (Zeiss) or LCS (Leica) software.

Nucleotide sequence accession number. The complete genome sequence of $HRSV^{B05}$ is available from GenBank under accession number KF640637.

RESULTS

Generation of a wild-type, subgroup B BA rHRSV. Total RNA was extracted directly from a tracheal rinse sample obtained from an infant infected with HRSV, and high-fidelity RT-PCR and rapid amplification of cDNA ends (RACE) were used to generate amplicons using previously described methods (29). The consensus genome sequence indicated that the virus belonged to the Buenos Aires (BA) genotype of HRSV subgroup B. This genotype was first detected in Argentina in 1999 and is characterized by a 60-nucleotide duplication in the G gene (30). Viruses of the BA genotype have become the dominant global HRSV subtype B genotype (31, 32), although why this is the case is unclear. Eukaryotic expression plasmids encoding $HRSV^{B05}$ nucleocapsid (N), phospho- (P), and M2-1 and large (L) proteins and a negative-sense minigenome ($HRSV^{B05}$DI-EGFP) were constructed (Fig. 1A), and a replication/transcription assay was established to optimize the conditions required to generate $rHRSV^{B05}$. Most negative-strand reverse genetics systems utilize T7 RNA polymerase to generate a full-length viral antigenomic RNA. Since T7 RNA polymerase initiates most efficiently on a stretch of guanine residues, efficient $rHRSV^{A2}$ rescue has previously been achieved by inserting three guanine nucleotides between the T7 promoter and the HRSV leader (Le) sequence (33–35). However, it is not clear whether this sequence is copied during viral replication. To negate this possibility, a hammerhead ribozyme (36) was inserted after the T7 promoter and three guanine nucleotides, which, along with the hepatitis delta ribozyme at the other end of the minigenome, allowed posttranscriptional cleavage to generate precise, authentic trailer (Tr) and Le termini at the ends of the minigenome (Fig. 1A). $EGFP^+$ cells were observed following transfection of the five plasmids into HEp-2 cells, indicating that the genomic termini and helper plasmids were functional (Fig. 1B). No EGFP-positive cells were observed when the L protein expression plasmid was omitted (Fig. 1B, −L), indicating that EGFP expression was driven exclusively by the viral RNA-dependent RNA polymerase (Fig. 1B). Based on these findings a positive-sense full-length genome plasmid ($pHRSV^{B05}$) was constructed, and $rHRSV^{B05}$ was recovered following transfection into HEp-2 cells (Fig. 1C). Importantly, it was not necessary to mutate nucleotide 4 of the Le sequence to achieve efficient rescue as has been described for $rHRSV^{A2}$ (33, 37), which demonstrates the biological importance of using authentic wild-type sequences. Full-genome consensus sequencing of the recombinant virus showed that no mutations had been introduced compared to the consensus sequence of the clinical specimen (data not shown). Indirect immunofluorescence (Fig. 1D and E) and *in situ* plaque staining (Fig. 1F and G) using an anti-HRSV F glycoprotein antibody permitted the detection of foci of infection. The full-length HRSV plasmid was modified by insertion of an ATU encoding EGFP at position 5 in the genome (Fig. 1H), and $rHRSV^{B05}$EGFP(5) was recovered (Fig. 1I). High levels of EGFP expression were obtained, and both single and fused infected cells were detected by UV microscopy (Fig. 1I). Thus, an $rHRSV^{B05}$ virus genetically identical to a clinical isolate was successfully generated that can be tracked in living cells in the absence of any overt CPE.

Growth characteristics of $rHRSV^{B05}$ in transformed and primary human cells. HEp-2 cells were infected with $rHRSV^{B05}$ or $rHRSV^{B05}$EGFP(5) at an equivalent multiplicity of infection (MOI). Both B05-based viruses displayed similar growth kinetics, reaching equivalent peak titers of 10^6 $TCID_{50}$/ml (Fig. 1J). It has been reported that HRSV strains differ in their binding affinity to glycosaminoglycan (GAG) moieties on the cell surface (19, 23). Both $rHRSV^{B05}$ and $rHRSV^{B05}$EGFP(5) displayed low GAG dependency indices (Fig. 1K). In contrast, rgRSV had a high GAG dependency index.

Primary NHBE cells were differentiated at ALI to form polarized ciliated, nonciliated, basal, and goblet cells with functional tight junctions. These wd-NHBE cells were infected at an MOI of 0.01, 0.1, or 1, resulting in a dose-dependent number of infected cells 2 d.p.i. (Fig. 2A). Similar to previous observations with recombinant HRSV A2 strains in differentiated epithelial cells (12), CPE was not observed. Virus loads in apical rinses were determined both by virus isolation (Fig. 2B) and qPCR (Fig. 2C). No reproducible differences in virus loads were determined between cultures infected with $rHRSV^{B05}$ and $rHRSV^{B05}$EGFP(5). Virus loads determined by qPCR showed a good correlation with the numbers of $EGFP^+$ cells. Neither released virus nor virus genome

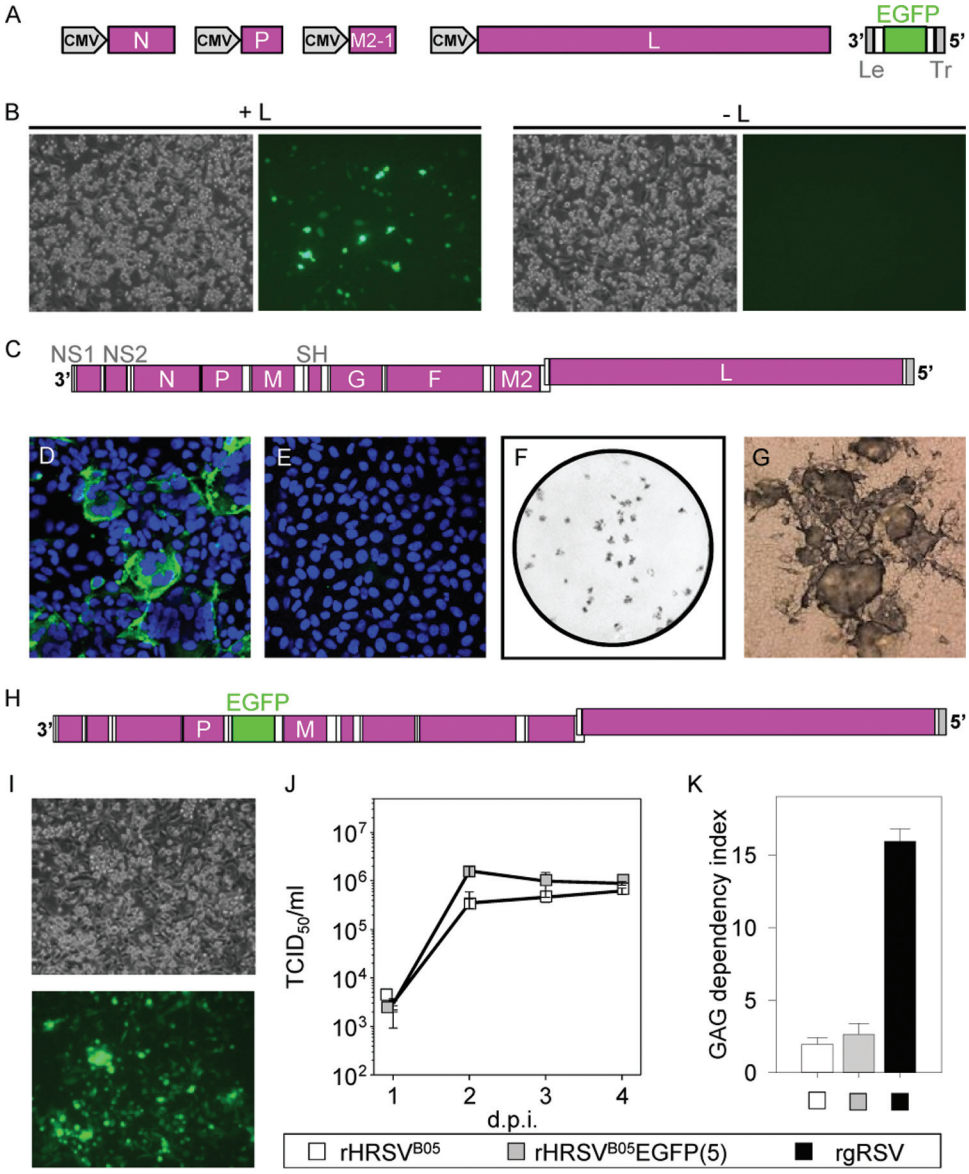

FIG 1 Development of a reverse genetics system for HRSV^{B05}. (A) Schematic representation of HRSV eukaryotic N, P, M2-1, and L protein expression constructs and minigenome HRSV^{B05}DI-EGFP showing the Le sequence, EGFP gene, and Tr sequence. (B) Phase-contrast and UV photomicrographs of HEp-2 cells at 2 days posttransfection with p(−)HRSV^{B05}DI-EGFP and helper plasmids with (+L) and without (−L) the L protein expression clone. (C) Schematic representation of the rHRSV^{B05} genome. (D and E) Detection of the F glycoprotein of rHRSV^{B05} syncytia by indirect immunofluorescence. A negative control omitted the primary monoclonal antibody (E). (F and G) Detection of HRSV^{B05} by immuno-plaque assay. (H) Schematic representation of the rHRSV^{B05}EGFP(5) genome. (I) Phase-contrast and fluorescent photomicrographs of rHRSV^{B05}EGFP(5)-infected HEp-2 cells. (J) Growth curves determined by 10-fold titrations at four consecutive days on HEp-2 cells. (K) CHO cells expressing GAG and cells deficient in GAG were infected, and ratios were calculated and expressed as a GAG index Data are presented as geometric mean titers ± standard errors. d.p.i., days postinfection; CMV, cytomegalovirus.

was detected in the basolateral compartment (data not shown). This is consistent with the epitheliotropic nature of HRSV.

rHRSV^{B05} efficiently infects cotton rats. Cotton rats were infected intranasally with 10^4 $TCID_{50}$ of rHRSV^{B05} or rHRSV^{B05}EGFP(5) in a low volume (10 μl) to target the URT. Animals were sacrificed at 4 or 6 d.p.i., and unfixed respiratory tracts were screened by UV microscopy. High numbers of EGFP$^+$ cells were detected at 4 d.p.i. in the nasal cavity of rHRSV^{B05}EGFP(5)-infected animals (Fig. 3A). Discrete tracks of fluorescent cells were present in the epithelium of the nasal septum, reminiscent of what was previously observed in wd-NHBE cells (12). No EGFP$^+$ cells were detected microscopically in trachea or lungs. Pathological assessment and immunohistochemistry (IHC) in 7-μm formalin-fixed lung sections indicated that both viruses predominantly infected ciliated respiratory epithelial cells (Fig. 3B) and caused destruction of the epithelium (Fig. 3C).

In order to target both the URT and LRT, cotton rats were intranasally infected with 10^4 $TCID_{50}$ in a larger volume (100 μl) (26). Macroscopically, fluorescence levels in the nasal concha and nasal septum were indistinguishable between animals infected with the low- or high-volume inoculum, and no EGFP$^+$ cells were

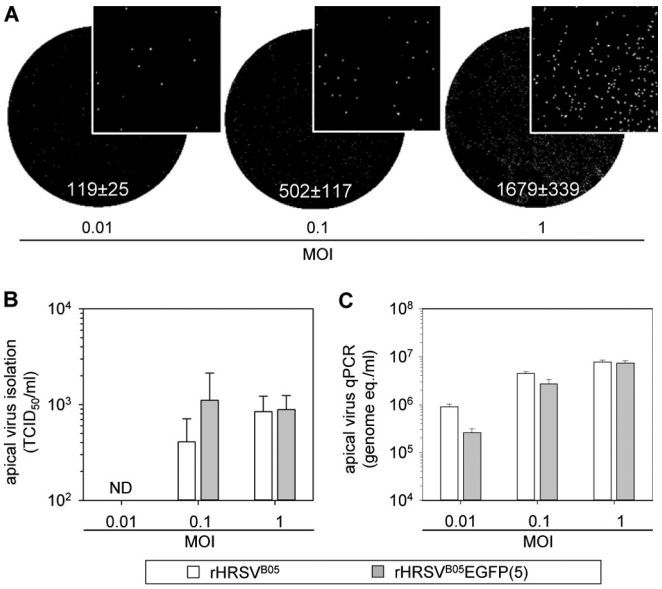

FIG 2 Infection of primary wd-NHBE cells grown at ALI with rHRSV^{B05} or rHRSV^{B05}EGFP(5). (A) Fluorescent photomicrographs and absolute counts of EGFP$^+$ cells/well for MOIs of 0.01, 0.1, and 1. (B) Virus isolations of corresponding apical rinses. (C) Genome equivalents in apical rinses measured by qPCR. Data are presented as geometric mean titers ± standard errors. ND, not determined.

detected in the trachea. However, vastly different outcomes were observed when the lungs from infected animals were removed, inflated with agarose, sectioned, and screened for fluorescence. Infection with rHRSV^{B05}EGFP(5) resulted in high numbers of EGFP$^+$ cells at 4 d.p.i. in the epithelium of the bronchi and bronchioles in the lung slices (Fig. 3D). The number of EGFP$^+$ cells in the LRT was lower at 6 d.p.i.

Virus loads were determined in nasal lavage samples (Fig. 3E and F) and lung tissue (Fig. 3G and H) by virus isolation (Fig. 3E and G) or qPCR (Fig. 3F and H) for animals infected with a low (Fig. 3, hatched columns) or high (Fig. 3, nonhatched columns) volume of intranasal inoculum. The results corroborated the macroscopic observations that high viral loads were detected in the URT of all animals (Fig. 3E and F) while only in animals inoculated with a high volume were significant virus loads detected in the LRT (Fig. 3G and H).

Detection of rHRSV^{B05}EGFP(5) in the respiratory tract by optical sectioning. The power of targeted pathology in understanding the spatial dynamics and pathological consequences of rHRSV^{B05}EGFP(5) infection is evident when standard IHC in 7-μm formalin-fixed lung sections (Fig. 4A and B) is compared with optical sectioning of living tissues immediately after necropsy (Fig. 4C to G). More infected cells were detected in agarose-inflated lung slices reconstructed in three dimensions using confocal laser scanning microscopy (CLSM) than by IHC, and sheets of infected luminal epithelial cells of bronchi and bronchioles were present (Fig. 4C). Small numbers of individual cells in the parenchyma of the lung were also present (Fig. 4C, inset and asterisk). These cells could not be phenotypically characterized by IHC due to the section size and lower level of sensitivity due to backgrounds. Optical sectioning also allows greater cellular resolution since EGFP floods the cytoplasm of the cell, meaning that fine processes and cell-to-cell contacts were readily visible (Fig. 4D and E, arrow).

DISCUSSION

We have developed a reverse genetics system based on an HRSV subgroup B clinical isolate and generated rHRSVs with or without an additional transcription unit encoding EGFP to study viral pathogenesis in the cotton rat model. Use of rHRSV^{B05}EGFP(5) allowed sensitive detection of infected cells both *in vitro* and *in vivo* in the early stages of infection in the absence of CPE. HEp-2 cells were suitable for virus passage *in vitro*, and the genomes were genetically stable: after 10 serial passages in HEp-2 cells, consensus sequencing revealed no mutations. In addition, the growth kinetics of rHRSV^{B05} and rHRSV^{B05}EGFP(5) were comparable, suggesting that insertion of an ATU into the HRSV genome did not result in virus attenuation. Laboratory-adapted viruses generated by extensive passage through a variety of disease-relevant and -nonrelevant cells and tissues have traditionally been used to develop molecular clones (34, 38–40).

HRSV spread in differentiated human airway epithelial (HAE) cells has been described as a "comet-like" spread, driven by the directionality of the beat of the cilia (12). Equivalent "comets" were present in the nasal conchae of infected cotton rats, demonstrating that these are relevant *in vivo* and not an *in vitro* artifact. Such localized virus spread has significant implications for the development and delivery of HRSV antivirals. We used the model to mirror the 1 to 2% of human cases where virus triggers bronchiolitis or severe pneumonia by varying the inoculation volume to target mainly the URT or concurrently the URT and LRT. Interestingly, rHRSV^{B05}EGFP(5) predominantly infected cells throughout the main branches of the bronchial tree, resulting in illumination of the bronchial tree. This aspect of HRSV pathogenesis has not previously been recapitulated in an animal model of HRSV or, to the best of our knowledge, in animals infected with any virus. Preferential infection of bronchial and bronchiolar epithelial cells mirrors the natural target cells of HRSV in humans (41). Moreover, at 4 d.p.i. rHRSV^{B05}EGFP(5) titers were similar to those obtained from patients or volunteers infected with HRSV (15, 16, 42). This illustrates the strength of the cotton rat model and shows the power of targeted pathology using EGFP-expressing recombinant viruses, which is only feasible due to the possibility of identifying infected tissues for blocking and processing immediately after necropsy.

Whereas existing *in vitro* and *in vivo* models of HRSV have focused mainly on subgroup A viruses, our recombinant virus is based on a subgroup B strain (31). Antigenic differences between the two subgroups of HRSV are predominantly mediated by the highly variable G gene (10) and might facilitate evasion of host immune responses (43). Despite these differences, infections with HRSV of either subgroup cause indistinguishable disease (1). Although outside the scope of understanding primary pathogenesis, this system should permit fitness experiments between viruses with and without the insertion in the G protein. This could explain why the BA viruses have outcompeted all other subgroup B HRSVs.

Reverse genetics of nonsegmented negative-strand RNA viruses has come a long way in the last 20 years following the recovery of rabies virus (44). The challenges of generating recombinant viruses are far from trivial, and much has been achieved with the original rHRSV systems (19, 34). Given the significant investment

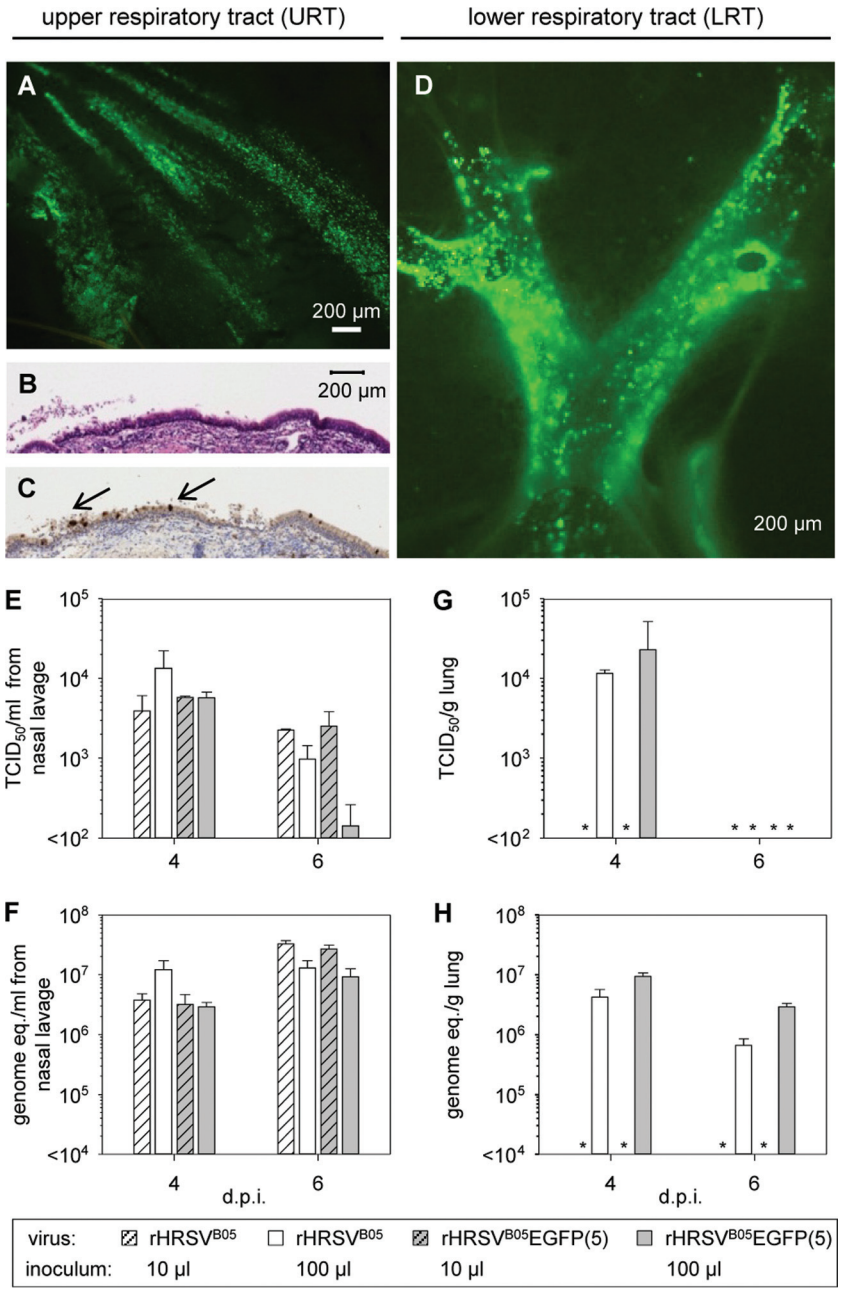

FIG 3 Intranasal infection of cotton rats with rHRSV^{B05} or rHRSV^{B05}EGFP(5). (A) Fluorescence microscopy showing high levels of infection in the nasal septum of cotton rats at 4 d.p.i. with rHRSV^{B05}EGFP(5), with comet-like formations of EGFP^{+} cells. (B and C) Hematoxylin and eosin staining and IHC photomicrographs of the tissues described in panel A showed destruction of epithelia (arrows). (D) In animals infected with a high (100 μl) inoculum large numbers of EGFP^{+} cells were also observed in the epithelium of bronchus and bronchioles, illuminating the bronchial tree. Virus loads were determined in nasal lavage samples (E and F) and lung tissue (G and H) by virus isolation (E and G) or qPCR (F and H) for animals infected with a low-volume (10 μl) or high-volume (100 μl) intranasal inoculum. Asterisks indicate virus loads lower than 10^2 $TCID_{50}$ (virus isolation) or 10^4 genome equivalents (qPCR) per gram of lung tissue.

of time in establishing reverse genetics systems, there tends to be a large activation energy required to develop second- or third-generation systems. This is particularly true for HRSV, and, although tractable second-generation systems have been developed (45, 46), no group has successfully generated a virulent rHRSV fully reflecting the sequence of a current, clinically relevant, wild-type strain and studied primary pathogenesis in this key small-animal model. In addition, *in vitro* and *in vivo* models employing subgroup B HRSV strains have been scarce; these will be of crucial importance for preclinical testing of the effectiveness of new intervention strategies. It is vital to extend ongoing studies and move in the direction of reverse genetics systems based on clinical isolates grown in disease-relevant cells. Only then will it be possible to understand HRSV pathogenesis fully and systematically to test novel interventions. The recombinant B05 viruses will help in this endeavor, and these

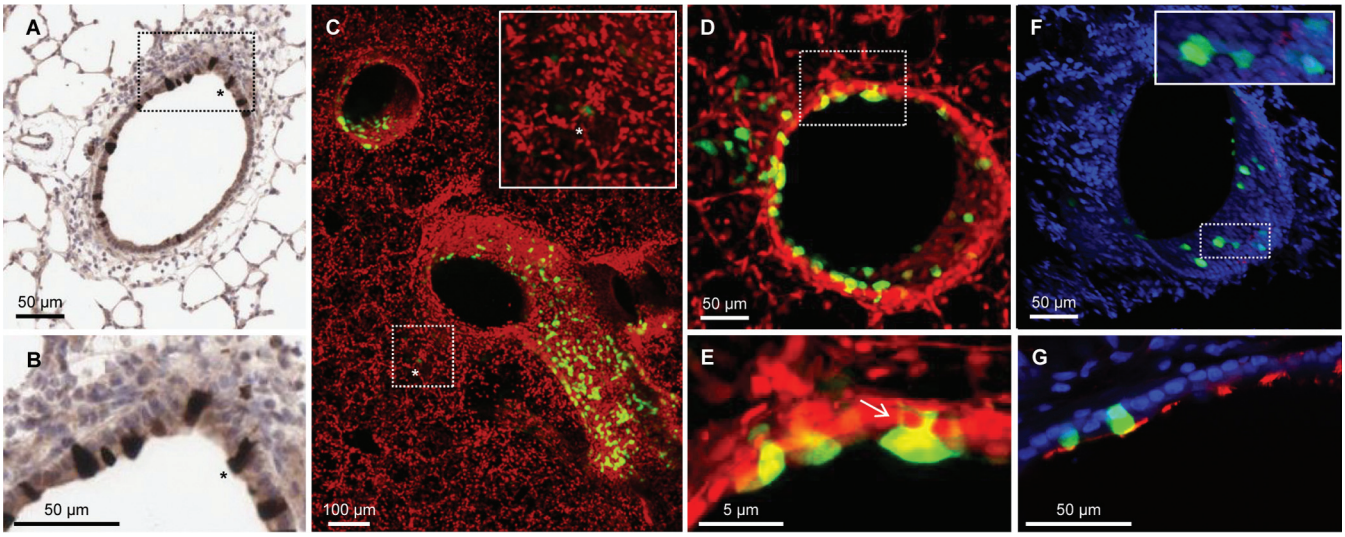

FIG 4 Microscopic imaging of rHRSV^{B05}EGFP(5) infection in cotton rats. (A and B) Standard IHC detection of rHRSV^{B05}EGFP(5) in 7-μm lung sections showing infected epithelial cells (asterisks). It is not possible to identify infected cells in the parenchyma convincingly. (C and D) Optical reconstruction of lung slices in three dimensions provides more information on the spatial orientation and infection in the LRT, and high numbers of infected cells (green) were visible; nuclei were counterstained (red). (E) Flooding of the cytoplasm of infected cells with EGFP (green) illuminated fine cellular processes (arrow). (F and G) High-resolution CLSM identified infected cells (F, green), which were β-tubulin positive (red) at the bronchiolar lumen (G); nuclei are counterstained (blue).

should be augmented by the establishment of equivalent systems for subgroup A clinical isolates.

ACKNOWLEDGMENTS

We thank Georgina Aron, Peter Coyle, Rory de Vries, Rachel Scheuer, and Joyce Verburgh. We thank Mark Peeples and Peter Collins for providing rgRSV as a positive control for the GAG index determination.

This work was funded by MRC (grant number G0801001) and the VIRGO Consortium, funded by the Dutch Government (grant number FES0908).

The funders had no role in study design, data collection and analysis, decision to publish, or preparation of the manuscript.

REFERENCES

1. **Collins PL, Karron RA.** 2013. Respiratory syncytial virus and metapneumovirus, p 1086–1123. *In* Knipe DM, Howley PM, Cohen JI, Griffin DE, Lamb RA, Martin MA, Rancaniello VR, Roizman B (ed), Fields virology, 6th ed. Lippincott Williams & Wilkins, Philadelphia, PA.
2. **Welliver R.** 2009. The relationship of meteorological conditions to the epidemic activity of respiratory syncytial virus. Paediatr Respir Rev **10**(Suppl 1):S6–S8. http://dx.doi.org/10.1016/S1526-0542(09)70004-1.
3. **Hall CB, Simoes EAF, Anderson LJ.** 2013. Clinical and epidemiological features of respiratory syncytial virus. Curr Top Microbiol Immunol **372:** 39–57. http://dx.doi.org/10.1007/978-3-642-38919-1_2.
4. **Collins PL, Melero JA.** 2011. Progress in understanding and controlling respiratory syncytial virus: still crazy after all these years. Virus Res **162:** 80–99. http://dx.doi.org/10.1016/j.virusres.2011.09.020.
5. **DeVincenzo JP, Aitken J, Harrison L.** 2003. Respiratory syncytial virus (RSV) loads in premature infants with and without prophylactic RSV fusion protein monoclonal antibody. J Pediatr **143:**123–126. http://dx.doi.org/10.1016/S0022-3476(03)00213-0.
6. **Graham BS.** 2011. Biological challenges and technological opportunities for respiratory syncytial virus vaccine development. Immunol Rev **239:** 149–166. http://dx.doi.org/10.1111/j.1600-065X.2010.00972.x.
7. **Krzyzaniak MA, Zumstein MT, Gerez JA, Picotti P, Helenius A.** 2013. Host cell entry of respiratory syncytial virus involves macropinocytosis followed by proteolytic activation of the F protein. PLoS Pathog **9:**e1003309. http://dx.doi.org/10.1371/journal.ppat.1003309.
8. **McLellan JS, Chen M, Leung S, Graepel KW, Du X, Yang Y, Zhou T, Baxa U, Yasuda E, Beaumont T, Kumar A, Modjarrad K, Zheng Z, Zhao M, Xia N, Kwong PD, Graham BS.** 2013. Structure of RSV fusion glycoprotein trimer bound to a prefusion-specific neutralizing antibody. Science **340:**1113–1117. http://dx.doi.org/10.1126/science.1234914.
9. **Johnson PR, Spriggs MK, Olmsted RA, Collins PL.** 1987. The G glycoprotein of human respiratory syncytial viruses of subgroups A and B: extensive sequence divergence between antigenically related proteins. Proc Natl Acad Sci U S A **84:**5625–5629. http://dx.doi.org/10.1073/pnas.84.16.5625.
10. **Tan L, Coenjaerts FE, Houspie L, Viveen MC, Van Bleek GM, Wiertz EJ, Martin DP, Lemey P.** 2013. The comparative genomics of human respiratory syncytial virus subgroups A and B: genetic variability and molecular evolutionary dynamics. J Virol **87:**8213–8226. http://dx.doi.org/10.1128/JVI.03278-12.
11. **Gray TE, Guzman K, Davis CW, Abdullah LH, Nettesheim P.** 1996. Mucociliary differentiation of serially passaged normal human tracheobronchial epithelial cells. Am J Respir Cell Mol Biol **14:**104–112. http://dx.doi.org/10.1165/ajrcmb.14.1.8534481.
12. **Zhang L, Peeples ME, Boucher RC, Collins PL, Pickles RJ.** 2002. Respiratory syncytial virus infection of human airway epithelial cells is polarized, specific to ciliated cells, and without obvious cytopathology. J Virol **76:**5654–5666. http://dx.doi.org/10.1128/JVI.76.11.5654-5666.2002.
13. **Villenave R, Thavagnanam S, Sarlang S, Parker J, Douglas I, Skibinski G, Heaney LG, McKaigue JP, Coyle PV, Shields MD, Power UF.** 2012. In vitro modeling of respiratory syncytial virus infection of pediatric bronchial epithelium, the primary target of infection in vivo. Proc Natl Acad Sci U S A **109:**5040–5045. http://dx.doi.org/10.1073/pnas.1110203109.
14. **Green MG, Huey D, Niewiesk S.** 2013. The cotton rat (*Sigmondon hispidus*) as an animal model for respiratory tract infections with human pathogens. Lab Anim (NY) **42:**170–176. http://dx.doi.org/10.1038/laban.188.
15. **Bagga B, Woods CW, Veldman TH, Gilbert A, Mann A, Balaratnam G, Lambkin-Williams R, Oxford JS, McClain MT, Wilkinson T, Nicholson BP, Ginsburg GS, Devincenzo JP.** 2013. Comparing influenza and RSV viral and disease dynamics in experimentally infected adults predicts clinical effectiveness of RSV antivirals. Antivir Ther **18:**785–791. http://dx.doi.org/10.3851/IMP2629.
16. **DeVincenzo JP, Wilkinson T, Vaishnaw A, Cehelsky J, Meyers R, Nochur S, Harrison L, Meeking P, Mann A, Moane E, Oxford J, Pareek R, Moore R, Walsh E, Studholme R, Dorsett P, Alvarez R, Lambkin-Williams R.** 2010. Viral load drives disease in humans experimentally infected with respiratory syncytial virus. Am J Respir Crit Care Med **182:** 1305–1314. http://dx.doi.org/10.1164/rccm.201002-0221OC.
17. **DeVincenzo JP, Whitley RJ, Mackman RL, Scaglioni-Weinlich C, Harrison L, Farrell E, McBride S, Lambkin-Williams R, Jordan R,**

Xin Y, Ramanathan S, O'Riordan T, Lewis SA, Li X, Toback SL, Lin SL, Chien JW. 2014. Oral GS-5806 activity in a respiratory syncytial virus challenge study. N Engl J Med **371:**711–722. http://dx.doi.org/10.1056/NEJMoa1401184.

18. **Falzarano D, Groseth A, Hoenen T.** 2014. Development and application of reporter-expressing mononegaviruses: current challenges and perspectives. Antiviral Res **103:**78–87. http://dx.doi.org/10.1016/j.antiviral.2014.01.003.
19. **Hallak LK, Collins PL, Knudson W, Peeples ME.** 2000. Iduronic acid-containing glycosaminoglycans on target cells are required for efficient respiratory syncytial virus infection. Virology **271:**264–275. http://dx.doi.org/10.1006/viro.2000.0293.
20. **Chambers P, Rima BK, Duprex WP.** 2009. Molecular differences between two Jeryl Lynn mumps virus vaccine component strains, JL5 and JL2. J Gen Virol **90:**2973–2981. http://dx.doi.org/10.1099/vir.0.013946-0.
21. **Lemon K, Rima BK, McQuaid S, Allen IV, Duprex WP.** 2007. The F gene of rodent brain-adapted mumps virus is a major determinant of neurovirulence. J Virol **81:**8293–8302. http://dx.doi.org/10.1128/JVI.00266-07.
22. **Reed LJ, Muench H.** 1938. A simple method of estimating fifty percent endpoints. Am J Hyg (Lond) **27:**493–497.
23. **Hallak LK, Kwilas SA, Peeples ME.** 2007. Interaction between respiratory syncytial virus and glycosaminoglycans, including heparan sulfate. Methods Mol Biol **379:**15–34. http://dx.doi.org/10.1007/978-1-59745-393-6_2.
24. **Verkaik NJ, Nguyen DT, de Vogel CP, Moll HA, Verbrugh HA, Jaddoe VW, Hofman A, Van Wamel WJ, van den Hoogen BG, Buijs-Offerman RM, Ludlow M, De Witte L, Osterhaus AD, van Belkum A, De Swart RL.** 2011. *Streptococcus pneumoniae* exposure is associated with human metapneumovirus seroconversion and increased susceptibility to *in vitro* HMPV infection. Clin Microbiol Infect **17:**1840–1844. http://dx.doi.org/10.1111/j.1469-0691.2011.03480.x.
25. **Dewhurst-Maridor G, Simonet V, Bornand JE, Nicod LP, Pache JC.** 2004. Development of a quantitative TaqMan RT-PCR for respiratory syncytial virus. J Virol Methods **120:**41–49. http://dx.doi.org/10.1016/j.jviromet.2004.03.017.
26. **Prince GA, Jenson AB, Horswood RL, Camargo E, Chanock RM.** 1978. The pathogenesis of respiratory syncytial virus infection in cotton rats. Am J Pathol **93:**771–791.
27. **Nguyen DT, De Vries RD, Ludlow M, van den Hoogen BG, Lemon K, Van Amerongen G, Osterhaus AD, De Swart RL, Duprex WP.** 2013. Paramyxovirus infections in *ex vivo* lung slice cultures of different host species. J Virol Methods **193:**159–165. http://dx.doi.org/10.1016/j.jviromet.2013.06.016.
28. **de Swart RL, Ludlow M, De Witte L, Yanagi Y, Van Amerongen G, McQuaid S, Yüksel S, Geijtenbeek TB, Duprex WP, Osterhaus AD.** 2007. Predominant infection of $CD150^+$ lymphocytes and dendritic cells during measles virus infection of macaques. PLoS Pathog **3:**e178. http://dx.doi.org/10.1371/journal.ppat.0030178.
29. **Rennick LJ, Duprex WP.** 2012. Modification of measles virus and application to pathogenesis studies, p 150–199. *In* Bridgen A (ed), Reverse genetics of RNA viruses: applications and perspectives. John Wiley & Sons, Chichester, United Kingdom.
30. **Trento A, Galiano M, Videla C, Carballal G, Garcia-Barreno B, Melero JA, Palomo C.** 2003. Major changes in the G protein of human respiratory syncytial virus isolates introduced by a duplication of 60 nucleotides. J Gen Virol **84:**3115–3120. http://dx.doi.org/10.1099/vir.0.19357-0.
31. **Trento A, Casas I, Calderon A, Garcia-Garcia ML, Calvo C, Perez-Brena P, Melero JA.** 2010. Ten years of global evolution of the human respiratory syncytial virus BA genotype with a 60-nucleotide duplication in the G protein gene. J Virol **84:**7500–7512. http://dx.doi.org/10.1128/JVI.00345-10.
32. **van Niekerk S, Venter M.** 2011. Replacement of previously circulating respiratory syncytial virus subtype B strains with the BA genotype in South Africa. J Virol **85:**8789–8797. http://dx.doi.org/10.1128/JVI.02623-10.
33. **Jin H, Clarke D, Zhou HZY, Cheng X, Coelingh K, Bryant M, Li S.** 1998. Recombinant human respiratory syncytial virus (RSV) from cDNA and construction of subgroup A and B chimeric RSV. Virology **251:**206–214. http://dx.doi.org/10.1006/viro.1998.9414.
34. **Collins PL, Hill MG, Camargo E, Grosfeld H, Chanock RM, Murphy BR.** 1995. Production of infectious human respiratory syncytial virus from cloned cDNA confirms an essential role for the transcription elongation factor from the 5′ proximal open reading frame of the M2 mRNA in gene expression and provides a capability for vaccine development. Proc Natl Acad Sci U S A **92:**11563–11567. http://dx.doi.org/10.1073/pnas.92.25.11563.
35. **Grosfeld H, Hill MG, Collins PL.** 1995. RNA replication by respiratory syncytial virus (RSV) is directed by the N, P, and L proteins; transcription also occurs under these conditions but requires RSV superinfection for efficient synthesis of full-length mRNA. J Virol **69:**5677–5686.
36. **Hammann C, Luptak A, Perreault J, de la Pena M.** 2012. The ubiquitous hammerhead ribozyme. RNA **18:**871–885. http://dx.doi.org/10.1261/rna.031401.111.
37. **Collins PL, Mink MA, Hill MG, Camargo IIIE, Grosfeld H, Stec DS.** 1993. Rescue of a 7502-nucleotide (49.3% of full-length) synthetic analog of respiratory syncytial virus genomic RNA. Virology **195:**252–256. http://dx.doi.org/10.1006/viro.1993.1368.
38. **Radecke F, Spielhofer P, Schneider H, Kaelin K, Huber M, Dotsch C, Christiansen G, Billeter MA.** 1995. Rescue of measles viruses from cloned DNA. EMBO J **14:**5773–5784.
39. **Ludlow M, Nguyen DT, Silin D, Lyubomska O, De Vries RD, von Messling V, McQuaid S, De Swart RL, Duprex WP.** 2012. Recombinant canine distemper virus strain Snyder Hill expressing green or red fluorescent proteins causes meningoencephalitis in the ferret. J Virol **86:**7508–7519. http://dx.doi.org/10.1128/JVI.06725-11.
40. **Luytjes W, Krystal M, Enami M, Parvin JD, Palese P.** 1989. Amplification, expression, and packaging of foreign gene by influenza virus. Cell **59:**1107–1113. http://dx.doi.org/10.1016/0092-8674(89)90766-6.
41. **Johnson JE, Gonzales RA, Olson SJ, Wright PF, Graham BS.** 2007. The histopathology of fatal untreated human respiratory syncytial virus infection. Mod Pathol **20:**108–119. http://dx.doi.org/10.1038/modpathol.3800725.
42. **El Saleeby CM, Bush AJ, Harrison LM, Aitken JA, Devincenzo JP.** 2011. Respiratory syncytial virus load, viral dynamics, and disease severity in previously healthy naturally infected children. J Infect Dis **204:**996–1002. http://dx.doi.org/10.1093/infdis/jir494.
43. **Sullender W.** 2000. Respiratory syncytial virus genetic and antigenic diversity. Clin Microbiol Rev **13:**1–15. http://dx.doi.org/10.1128/CMR.13.1.1-15.2000.
44. **Schnell MJ, Mebatsion T, Conzelmann KK.** 1994. Infectious rabies viruses from cloned cDNA. EMBO J **13:**4195–4203.
45. **Hotard AL, Shaikh FY, Lee S, Yan D, Teng MN, Plemper RK, Crowe JE, Jr, Moore ML.** 2012. A stabilized respiratory syncytial virus reverse genetics system amenable to recombination-mediated mutagenesis. Virology **434:**129–136. http://dx.doi.org/10.1016/j.virol.2012.09.022.
46. **Widjojoatmodjo MN, Boes J, Van Bers M, Van Remmerden Y, Roholl PJM, Luytjes W.** 2010. A highly attenuated recombinant human respiratory syncytial virus lacking the G protein induces long-lasting protection in cotton rats. Virol J **7:**114. http://dx.doi.org/10.1186/1743-422X-7-114.